International Journal of Minerals, Metallurgy and Materials
Volume 27, Number 5, May 2020, Page 693
https://doi.org/10.1007/s12613-019-1933-3

Effects of chelating agents on the sol−gel synthesis of nano-zirconia: Comparison of the Pechini and sugar-based methods

Faramarz Kazemi[1)], *Farzin Arianpour*[2)], *Mahdiar Taheri*[3)], *Ali Saberi*[4)], *and Hamid Reza Rezaie*[5)]

1) Department of Mining and Metallurgy, Amirkabir University of Technology, Tehran, Iran
2) Research and Application Center, Kastamonu University, Kastamonu, Turkey
3) College of Engineering and Computer Science, The Australian National University, Canberra, Australia
4) Materials Processing, Faculty of Engineering Science, University of Bayreuth, Bayreuth, Germany
5) School of Metallurgy and Materials Engineering, Iran University of Science and Technology, Tehran, Iran
(Received: 16 June 2019; revised: 16 October 2019; accepted: 25 October 2019)

Abstract: This study focused on the comparison of the Pechini and sugar-based combustion synthesis methods to produce nano-zirconia. Zirconium hydroxide was utilized as metal precursor and citric acid, sucrose, and fructose were used as chelating agents, followed by calcination at 500, 600, and 700°C in air, respectively. Characterization was conducted by thermal analysis, specific surface area measurement, Fourier transform infrared spectroscopy, X-ray diffraction, and scanning and transmission electron microscopy. When sucrose and citric acid were used as chelating agents during synthesis, mixtures of monoclinic and tetragonal phases were formed after calcination at 600 and 700°C. In the fructose samples, the tetragonal structure was the unique characterized phase. The tetragonal parameters in the fructose samples were determined using the diffraction data and the lattice parameter ratio was proven to increase with the temperature increase. Compared with the citrate and sucrose samples, the largest specific surface area (27 $m^2 \cdot g^{-1}$) and smallest particle size (39.1 nm) were obtained for the fructose sample after calcination at 700°C. The study revealed the formation of single-phase stabilized tetragonal zirconia using fructose as chelating agent after calcination at 500°C, and the presence and formation mechanism of stabilized tetragonal phase were also discussed on the basis of the X-ray and electron diffraction studies.

Keywords: zirconia; nanopowder; sol−gel; sugar; Pechini; chelation

1. Introduction

Wet chemical methods based on hydroxide precipitation from salt or alkoxide hydrolysis are effective routes to produce oxide nanopowders [1]. Among these methods, sugar-based acid-catalyzed sol−gel synthesis is a technique commonly used for ceramic nanopowders [2]. In this route, different sugars (e.g., sucrose, maltose, fructose, or glucose) are generally used as seeding templates to synthesize nano-oxides with tailored pore size [3]. Sugar acts as a chelating agent to homogenously trap ions in the solution through a process involving the dehydration of metal complexes, followed by the decomposition of sugar [2,4]. After dehydration, a dark gel is obtained. Then, after heat treatment in air, a nanopowder is produced. In this case, the degree of porosity has a direct relationship with the amounts of gases that are generated during the process [2–5]. The Pechini (citrate-based) route is developed to avoid some disadvantages of conventional methods, such as inhomogeneity [6]. The aim of this technique is to obtain a uniform mixture through the chelation of metal cations using a hydroxycarboxylic acid, e.g., citric acid [6−7]. Through heat treatment after chelation, the mixture is transformed into a gel, excess water is removed, and polyesterification is induced [7]. Finally, the polymeric gel is calcined at relatively high temperatures to remove all residual organic matters [6–9]. The preparation of nano-zirconia using sucrose [10−11], maltose [12], glucose/fructose [13], and citric acid [14–17] has been reported. A brief overview of recent research is presented in Table 1. In this table, c, t and m represent cubic, tetragonal and monoclinic zirconia phases respectively; *T* is temperature, and CS is crystallite size.

Several zirconium sources (e.g., nitrate [12,18], oxynitrate [15,19], chloride [3,20], oxychloride [10,16,21], isopropoxide [20,22–24], *n*-butoxide [13], and acetylacetonate [14,17]) have been used for the synthesis of nano-zirconia.

Corresponding author: Hamid Reza Rezaie E-mail: hrezaie@iust.ac.ir

Most of these compounds are generally expensive, flammable/explosive, toxic, and potentially harmful to humans or the environment. In this work, zirconium hydroxide was used as a precursor, and citric acid, sucrose and fructose were utilized as chelating agents to synthesize nano-tetragonal zirconia after calcined at 500, 600, and 700°C, respectively. These chelating agents are considered green materials, which are not dangerous. The effects of these chelating agents on gel formation, thermal decomposition, and nanopowder characteristics were investigated by thermal analysis (i.e., differential thermal analysis (DTA)/thermogravimetric (TG) tests), Fourier transform infrared spectroscopy (FT-IR), specific surface area measurement, Raman spectroscopy, X-ray diffraction (XRD), and scanning and transmission electron microscopy (SEM/TEM).

Table 1. Nano-tetragonal zirconia synthesis via sugar-based and Pechini methods

Precursor	Chelating agent	T / °C	Phase	CS / nm	Reference
Oxychloride	Sucrose	600	c	6–10	[10]
Acetylacetonate	Sucrose	490	t	12.7–33.5	[11]
Nitrate	Maltose	500	t	—	[12]
Isopropoxide	Glucose/fructose	700	t, m	16–23	[13]
Oxynitrate	Citric acid	600	t	9	[14]
Oxychloride	Citric acid	700	t	10.2–32.9	[15]
Oxynitrate	Citric acid	625	t, c	12.5–14.8	[16]
Acetylacetonate	Citric acid	490	t	13.4	[17]

2. Experimental

2.1. Materials

Zirconium hydroxide was used as zirconium precursor. This powder was previously synthesized via a facile, green, and economical roast-leach method from commercially available zircon sand [25]. This powder has a chemical purity of >99.5wt% and is easily soluble in nitric acid. Chemical grade sucrose, fructose, and citric acid were selected as chelating agents. Other chemicals used in this study were nitric acid (65wt%), ammonia solution (25wt%), and polyvinyl alcohol (PVA, molecular weight = 1.6×10^5 g·mol^{-1}). All purchased chemicals were used as received without any further purification. The characteristics of the used chemicals are listed in Table 2.

Table 2. Characteristics of the used chemical materials

Material	Formula	Function	Catalogue No.	Supplier
Zirconium hydroxide	$Zr(OH)_4$	Precursor	—	—
Sucrose	$C_{12}H_{22}O_{11}$	Chelating agent	S9378	Sigma-Aldrich, USA
Fructose	$C_6H_{12}O_6$	Chelating agent	239704	Sigma-Aldrich, USA
Citric acid	$C_6H_8O_7{\cdot}H_2O$	Chelating agent	100247	Merck, Germany
Nitric acid	HNO_3	Solvent	100441	Merck, Germany
Ammonia	NH_4OH	pH adjustment	105432	Merck, Germany
Polyvinyl alcohol	$(C_2H_4O)_x$	Polymerization agent	363065	Sigma-Aldrich, USA

2.2. Synthesis

In the Pechini method, the molar ratio of citric acid to zirconium hydroxide was adjusted to 0.5:1. Zirconium hydroxide was dissolved into nitric acid. Then, citric acid was added during mixing at 80°C for 2 h. Citric acid acts as a chelating agent (to bind zirconium ions and inhibit precipitation during pH value adjustment) and a fuel to induce reactions. The pH value of the solution was adjusted to 6 by dropwise adding ammonium hydroxide solution. The mixture was stirred at 120°C for 4 h and dried in an electric oven at 180°C for 4 h to transform into a gel. In the sugar-based method, the stoichiometric mole ratio of zirconium hydroxide, sugar, and PVA was adjusted to 1:4:0.5 for sucrose and 1:8:0.5 for fructose. Sols were prepared by dissolving zirconium hydroxide and PVA in nitric acid, adding sucrose/fructose to the solutions, and mixing at 80°C for 2 h. The pH value was adjusted to 1 by dropwise adding diluted nitric acid and mixing continued for an additional 4 h. Then, the sols were dried at 200°C for 4 h in the electric oven. All prepared gels were gently powdered and micronized using an agate mill and passed through a 325 mesh (44 μm) sieve to produce homogenous powders and break large agglomerates. Then, samples were poured into alumina crucibles and calcined at 500, 600, and 700°C for a soaking time of 1 h in an electric furnace in air, respectively. The calcination temperatures were selected on the basis of the thermal analysis results. The flowcharts of the Pechini and sugar-based methods are shown in Figs. 1(a) and 1(b), respectively.

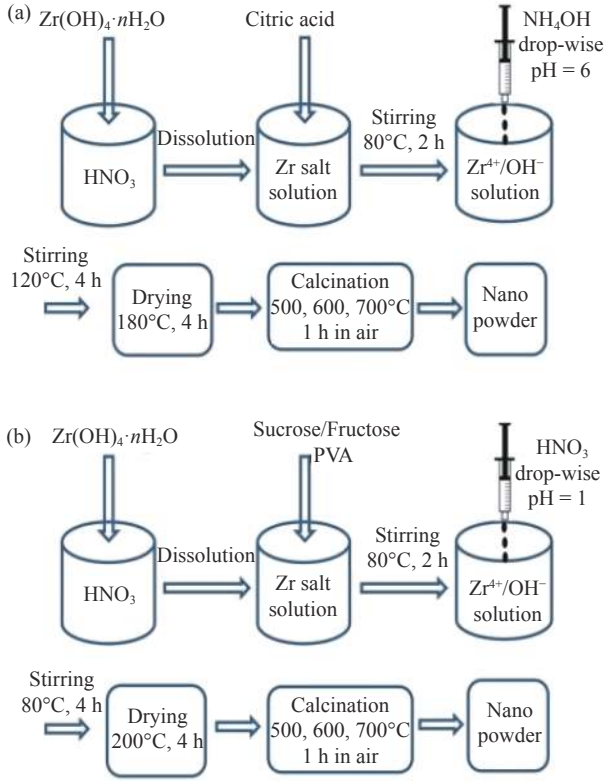

Fig. 1. Nano-zirconia synthesis via (a) Pechini and (b) sugar-based methods.

2.3. Characterization

DTA and TG tests were conducted on a 449-C thermal analyzer (Netzsch, Germany) equipped with an alumina cell at a heating rate of 10°C·min^{-1} up to 750°C in air. The FT-IR spectra were recorded in the range of 400–4000 cm^{-1} using an IR spectrometer (Shimadzu, Japan). Pellets were prepared by pressing a mixture of spectral grade KBr and 1wt% of samples. Raman spectroscopy was performed at room temperature using a LabRAM system (Horiba, Japan). The samples were excited with a 532 nm laser, and the spectrum was obtained via a silicon charge-coupled device detector. The phase composition was monitored by XRD on an AXS-2002 diffractometer (Bruker, USA) using Ni-filtered Cu $K_{\alpha 1}$ radiation (λ = 0.15406 nm) in the 2θ range of 10° to 70°, step size of 0.02°, time per step of 1 s, and generator setting of 40 kV, 40 mA at room temperature. The apparent crystallite sizes were measured according to the Scherrer equation (Eq. (1)) [26]. In this formula, λ is the X-ray wavelength, θ_0 is the Bragg angle, N is a constant (0.9), and CS is the apparent crystallite size in nm. $\beta(2\theta)$ is the peak full width at half maximum (FWHM) intensity in rad, which was taken as the experimental full width (β_{exp}) and corrected for the experimental instrumental broadening (β_{ins}) according to Eq. (2) [27]. The β_{ins} parameter was measured experimentally using silicon. The volume percentages of monoclinic (V_m) and tetragonal (V_t) phases were determined according to Eqs. (3) and (4), respectively [14,28–29]. In Eq. (3), parameters I_m and I_t indicate the X-ray peak intensity of the monoclinic and tetragonal crystalline plane. Eq. (5) was used to calculate the lattice parameters of the tetragonal zirconia phase [26], and h, k, and l are the crystalline plane indices, a and c are the tetragonal crystal lattices (nm), and d is the crystalline plane distance (nm).

$$\beta(2\theta) = \frac{N\lambda}{\mathrm{CS}\cdot\cos\theta_0} \tag{1}$$

$$\beta(2\theta) = \left(\beta^2_{\mathrm{exp}} - \beta^2_{\mathrm{ins}}\right)^{1/2} \tag{2}$$

$$X_m = \frac{I_m\left(\bar{1}11\right) + I_m(111)}{I_m\left(\bar{1}11\right) + I_m(111) + I_t(101)} \tag{3}$$

$$\begin{cases} V_m = \dfrac{1.311X_m}{1+0.311X_m}\times 100\% \\ V_t = (1-V_m)\times 100\% \end{cases} \tag{4}$$

$$\frac{1}{d^2} = \frac{h^2+k^2}{a^2} + \frac{l^2}{c^2} \tag{5}$$

Specific surface area was measured using the N_2 physisorption and Brunauer-Emmett-Teller (BET) methods at −196.15°C on a Gemini ASAP-2010 (Micromeritics, USA) system using ultrapure nitrogen gas. To remove the absorbents, the samples were degassed at 100°C for 2 h under vacuum before the test. The particle sizes (PS, nm) were derived using Eq. (6), where $\tilde{n}$ is the theoretical density of zirconia (5.68 g·cm^{-3}) and S refers to the specific surface area of the samples in m^2·g^{-1} [30].

$$\mathrm{PS} = \frac{6000}{\tilde{n}S} \tag{6}$$

The microstructural and morphological features were observed using a LEO-1530 field emission scanning electron microscope (Gemini FEG FE-SEM, Zeiss, Germany). To prepare the samples, the powders were ultrasonically dispersed into isopropanol and a drop of suspension was spread on an aluminum plate by a syringe. Then, the samples were sputter coated with a thin gold-platinum layer to prevent electron charging. A LIBRA 200 transmission electron microscope (TEM, Zeiss, Germany) with a 200 kV accelerating voltage was utilized for further high-resolution imaging and electron diffraction. A diluted sol was prepared by ultrasonically dispersing the powders into isopropanol, spreading a small drop on a 200 mesh copper grid, drying, and covering with an amorphous carbon film.

3. Results and discussion

3.1. Thermal behavior

Figs. 2(a) and 2(b) show the thermal analysis curves (DTA and TG) of the prepared gels via the Pechini and sugar-based methods using citric acid, sucrose, and fructose as chelating agents. The DTA curves plotted in Fig. 2(a) show a

sharp exothermic peak at 233°C for the citric acid (citrate) gel, which is related to the decomposition of ammonium nitrate formed during gel preparation via the Pechini method [27]. The weight loss behavior of sucrose shows a slightly different behavior compared with the other chelating agents and occurs in one step. It can be attributed to the complex structural and molecular changes of chelating agents, particularly for sugar molecules, such as oxidation changes of the functional groups with the increase in temperature [4,27]. The enthalpies of the reactions (released heat) using different chelating agents were calculated by measuring the area of the related DTA curves on the basis of the unit of measure (i.e., $J \cdot g^{-1}$) of the sample. For the Pechini process, the combustion was achieved in the temperature range from 200 to 650°C and the enthalpy was equal to 20.26 $J \cdot g^{-1}$. Clearly, most of the heat was released at approximately 230°C, which might affect and increase the final particle sizes of the synthesized nanopowders. The combustion of sucrose and fructose gels was completed before 555°C with the enthalpy values of 19.91 and 14.71 $J \cdot g^{-1}$, respectively. The TG curves plotted in Fig. 2(b) show that weight loss of all gels gradually starts at approximately 150°C; however, it stops for the citrate gel at a higher temperature (670°C) than the sugar-based gels (550°C). Clearly, the decomposition of sucrose gel led to 83.5wt% weight loss, whereas the decomposition of fructose and citrate gels led to approximately 71.1wt% and 82.1wt% weight loss, respectively. The mass losses during heating of the sugar-based gels are attributed to the decomposition of the organic chelating agents (sucrose and fructose) and the combustion of the polymeric matrix (PVA) [10,13].

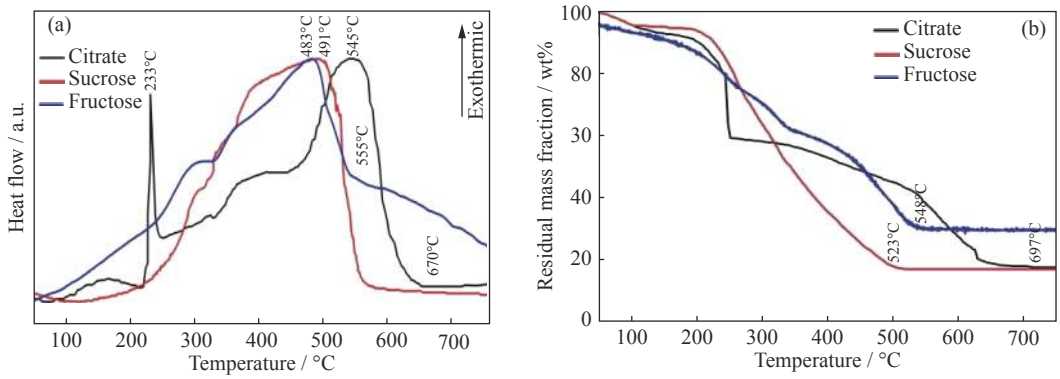

Fig. 2. Thermal analysis curves of the gels: (a) DTA and (b) TG.

In the sugar-based synthesis of nano-zirconia, the released gases due to the decomposition of the chelating agents produce a porous structure in the final powder [1]. The existing nitric acid in the starting sol leads to the hydrolysis of sugar molecules and the formation of primary fragments, such as D-glucose or D-fructose. These basic sugar molecules have the same molar weight and chemical formula, with different ring-type molecular structures. The decomposition energy of these sugar molecules is also enough to induce the synthesis reaction; meanwhile, their free alcohol easily functions and homogenously traps metal cations in the produced gels [2–5]. Synthesized powders from wet chemical techniques are generally amorphous and easily crystallize [6–7]. In the Pechini technique, which is based on the citrate-nitrate reaction, metal ions are trapped in the homogeneous gel mixture, which finally leads to the formation of molecular-scale nano-oxide materials with a uniform composition [8]. Releasing the exothermic energy of the metal–citrate complex induces the reaction and reduces the crystallization temperature of nano-zirconia particles [6–9].

3.2. Phase characteristics

Fig. 3 shows the XRD patterns of the synthesized nano-zirconia powders using sucrose, fructose, and citric acid as chelating agents and calcined at 500, 600, and 700°C for 1 h in air. For the citrate sample calcined at 500°C, the main phase is composed of monoclinic zirconia. Some small peaks related to the remaining ammonium nitrate from the Pechini process are also visible in the phase composition of the citrate sample, but this phase disappears when heating the gel at 600 and 700°C. This finding indicates that 500°C is insufficient to induce the synthesis reaction in this process using citric acid as chelating agent. In the sucrose sample calcined at 500°C, the phase composition is a mixture of tetragonal and monoclinic zirconia, while in the fructose sample calcined at 500°C, the XRD pattern only shows the presence of the tetragonal phase. After calcination at 600 and 700°C, mixtures of the tetragonal and monoclinic phases are visible in both citrate and sucrose samples, but tetragonal zirconia is still the unique phase for the fructose sample. In fact, using XRD technique, the main characteristic peak of tetragonal zirconia related to (102) plane could not be observed because of peak broadening phenomena in nanocrystalline materials; so the tetragonal phase could not be distinguished from cubic phase, which is the main disadvantage of XRD technique for phase determining of zirconia nanopowder [31–32]. Hence, in this work, electron diffraction using TEM was employed as the main characterization technique to validate the formation of

pure tetragonal zirconia phase for the fructose sample, which is discussed below. Table 3 shows the phase composition and diffraction data of the samples calcined at different temperatures. In this table, T is the calcination temperature, V is the phase volume fraction, CS is the crystallite size, $\beta(2\theta)$ is the full width at half maximum of 2θ, and t and m represent the tetragonal and monoclinic phases of zirconia, respectively.

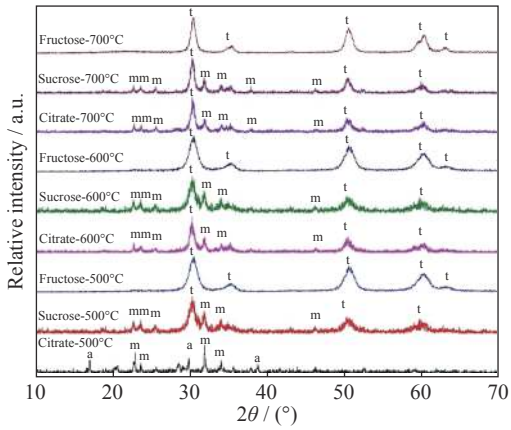

Fig. 3. X-ray diffraction patterns of the calcined powders (t: tetragonal zirconia; m: monoclinic zirconia; a: ammonium nitrate).

For the citrate sample, the XRD patterns indicate that, although the monoclinic phase started to form at 500°C, a high volume fraction of zirconia was crystallized in tetragonal form during heating at 600 and 700°C. For the sucrose sample, the crystallization of both monoclinic and tetragonal phases started at 500°C and the crystallization of the tetragonal phase exhibited an increase trend with the increase of the calcination temperature. The XRD patterns of the fructose sample calcined at different temperatures show that tetragonal zirconia is the unique phase and there is no evidence of the monoclinic phase. This finding can be attributed to the high fraction of crystallization in the amorphous phase for the fructose sample [33]. From Table 3, the sample prepared with fructose has the smallest crystallite size at 500°C compared with the other samples and the crystallite size of the samples increases with the increase of the calcination temperature [34]. The fructose sample calcined at 700°C has the largest crystallite size of tetragonal zirconia.

Table 4 presents the lattice parameters of the tetragonal phase of the fructose sample calcined at 500, 600, and 700°C calculated using Eq. (5). In this table, 2θ is the diffraction angle, (hkl) is the crystalline plane index, and d is the crystalline plane distance. Parameters a_c and c_c are the calculated lattice parameters of the tetragonal phase (nm), which are compared with the theoretical values of a_r (0.3592(5) nm) and c_r (0.5183(7) nm) as reference data obtained from the XRD card of the tetragonal zirconia phase (JCPDS-80-0965). The numbers in the parentheses show the approximation of the last digits in the calculations. These data were used to plot Fig. 4, which shows that the c_c/a_c ratio for the tetragonal phase increased with the increase of temperature. As shown above, the crystallite sizes increased with the increase of temperature. The strain of the tetragonal crystal lattice is caused by the applied surface tension of the nanoscale synthesized grains and related to the crystallite size [35], which means that when the crystallite size increased, the strain decreases; therefore, the c_c/a_c factor of the unit cell increases. However, with calcination in lower temperatures, which produce smaller crystallites, the cell structure would be under more strain, leading to the decrease in the c_c/a_c ratio which causes the small observed difference between calculated and reference crystal parameters of the tetragonal phase according to standard card (00-042-1164).

3.3. Specific surface area and particle size

Table 5 shows the specific surface areas and particle sizes of the synthesized nano-zirconia powder using different chelating agents and calcined at 500, 600, and 700°C for 1 h. In

Table 3. Phase composition and diffraction data

Sample	T / °C	Phase	V / %	(hkl)	2θ / (°)	$\beta(2\theta)$ / rad	CS / nm
Sucrose	500	t	66	(101)	30.273	0.820	9.2
		m	34	$(\bar{1}11)$	31.760	0.396	20.8
Fructose		t	~100	(101)	30.478	1.170	7.02
Citrate		m	~100	$(\bar{1}11)$	31.842	0.131	63.1
Sucrose	600	t	67	(101)	30.269	0.550	15.8
		m	33	$(\bar{1}11)$	31.762	0.360	22.9
Fructose		t	~100	(101)	30.382	0.650	12.6
Citrate		t	71	(101)	30.180	0.491	16.8
		m	29	$(\bar{1}11)$	31.842	0.389	21.5
Sucrose	700	t	74	(101)	30.243	0.520	15.9
		m	26	$(\bar{1}11)$	31.775	0.270	30.6
Fructose		t	~100	(101)	30.466	0.360	22.9
Citrate		t	72	(101)	30.223	0.412	21.4
		m	28	$(\bar{1}11)$	31.808	0.304	27.2

Table 4. Lattice parameters of the tetragonal zirconia phase for the fructose sample

T / °C	(hkl)	2θ / (°)	d / nm	a_c / nm	c_c / nm
500	(011)	30.4671	0.293407	0.3589(6)	0.5113(9)
	(112)	35.2359	0.254713	0.3592(2)	0.5138(3)
	(110)	50.6223	0.180322	0.3602(2)	0.5081(9)
600	(011)	30.4659	0.293417	0.3575(6)	0.5135(0)
	(112)	35.3633	0.253825	0.3584(4)	0.5155(5)
	(110)	50.5245	0.180498	0.3585(1)	0.5113(9)
700	(011)	30.3836	0.294193	0.3561(6)	0.5135(0)
	(112)	35.3367	0.254010	0.3584(4)	0.5149(9)
	(110)	50.4700	0.180830	0.3585(1)	0.5131(4)

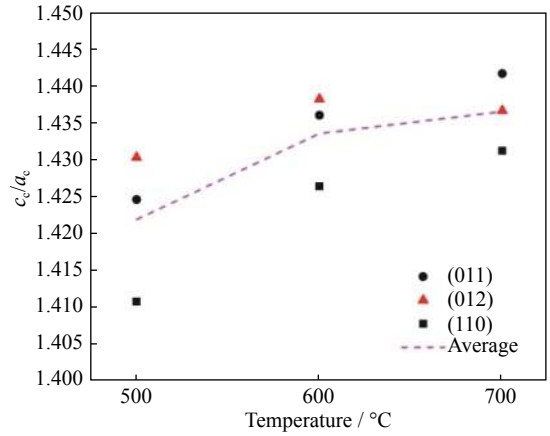

Fig. 4. Lattice parameter ratio vs. temperature of the tetragonal zirconia phase for the fructose sample.

this table, S is the specific surface area and PS is the particle size of the samples. For the fructose and sucrose samples, with the increase of the calcination temperature, the specific surface area decreases and the particle size increases. For the citrate sample, the trend is different: the largest particle size (96 nm) and smallest specific surface area (11 $m^2 \cdot g^{-1}$) are observed after calcination at 500°C; with the calcination temperature increase to 600°C, the particles size decreases drastically and the specific surface area increases; but after calcination at 700°C, the particle size increases and specific surface area decreases. After calcination at 700°C, compared with the other samples, the fructose sample has the largest specific surface area (27 $m^2 \cdot g^{-1}$) and smallest particle size (39.12 nm).

In the sugar-based synthesis method using sucrose as chelating agent, the addition of nitric acid induces the decomposition of sucrose molecules into glucose and fructose, which then prevents the recrystallization of sugar molecules. Releasing the functional groups of the decomposed products leads to bond formation between metallic ions in the homogeneous solution, which reduces the chance of precursor precipitation [2–5]. Through the heating process, the metal-ion-chelated complex is decomposed into carbon dioxide and water; meanwhile, a large amount of heat is generated. This phenomenon produces gases that inhibit particle agglomeration and help form pores and high surface area particles [36]. Costa *et al.* [31] investigated the difference between the pore size distributions of the samples produced using sucrose and fructose as template materials. Their results revealed a heterogenous pore size distribution for sucrose and a homogenous pore size distribution for fructose. The wide pore size range of the samples produced using sucrose results in particles with different size distributions and leads to the simultaneous formation of monoclinic and tetragonal phases [13–14,34]. This would probably be the main reason for the largest specific surface area and smallest particle size of the fructose sample after calcination at 700°C. The thermal analysis results (DTA curves plotted in Fig. 2(a)) indicate that a large amount of heat was released from the citrate gel during heating at approximately 230°C. Clearly the formation of zirconia would not be completed before 500°C. The large crystallite size and small surface area of the citrate sample calcined at 500°C are an evidence for such a claim. With the increase in the calcination temperature to 600°C and the completion of the reaction, the particle size decreased drastically and the specific surface area increased. However, after calcination at 700°C, the particle size and specific surface area logically increased and decreased, respectively. This observation is consistent with the XRD data.

Zhang *et al.* [33] conducted a research on the particle size dependency and phase stability of nano-sized zirconia. Both of their experimental results and theoretical calculations indicated that tetragonal zirconia nanoparticles with PS < 14 nm were thermodynamically stable at room temperature and

Table 5. Specific surface areas (S) and particle sizes (PS) of the nano-zirconia powders

T / °C	S / ($m^2 \cdot g^{-1}$)			PS / nm		
	Sucrose	Fructose	Citrate	Sucrose	Fructose	Citrate
500	86	94	11	12.3	11.2	96
600	29	35	26	36.4	30.1	40
700	21	27	23	50.3	39.1	46

the nanoparticles with 14 < PS < 31 nm were metastable probably because of a kinetic nucleation barrier. From Table 5, only the particle size of the tetragonal phase in the fructose sample calcined at 500°C is smaller than 14 nm. Thus, using fructose as chelating agent and calcining at the lower temperature of 500°C seems to be a more effective route to produce tetragonal zirconia phase.

3.4. Spectroscopy

Fig. 5(a) shows the FT-IR spectra of the nanopowders synthesized using different chelating agents and calcined at 700°C. The wide band observed in the frequency range of 3100–3550 cm^{-1} and the narrow band observed in the frequency range of 1640–1650 cm^{-1} are attributed to the stretching and bending vibrations of the O–H groups due to the absorbed water molecules from the air. Another narrow band observed in the frequency range of 2340–2360 cm^{-1} is ascribed to the coupling effect of the stretching and bending vibrations of –OH groups. Stretching of the Zr–O crystalline bands indicates absorption at low frequencies. The wide absorption band and corresponding shoulder at 608–639 cm^{-1} is assigned to the Zr–O vibration of the tetragonal phase. The narrow band in the range of 982–993 cm^{-1} is attributed to the monoclinic phase in the FT-IR spectra of the sucrose and citrate samples. These findings are consistent with the XRD data. Similar observations were also reported for the FT-IR analysis of the zirconia nanoparticles [11,13]. Fig. 5(b) shows the Raman spectrum of the fructose-based sample heated at 700°C and illustrates the positions of the peaks of the tetragonal zirconia phase. However, the differences between cubic and tetragonal phase of zirconia could not be distinguished using Raman spectroscopy, which is the same problem as using the XRD technique because of the same patterns obtained for them [31–32].

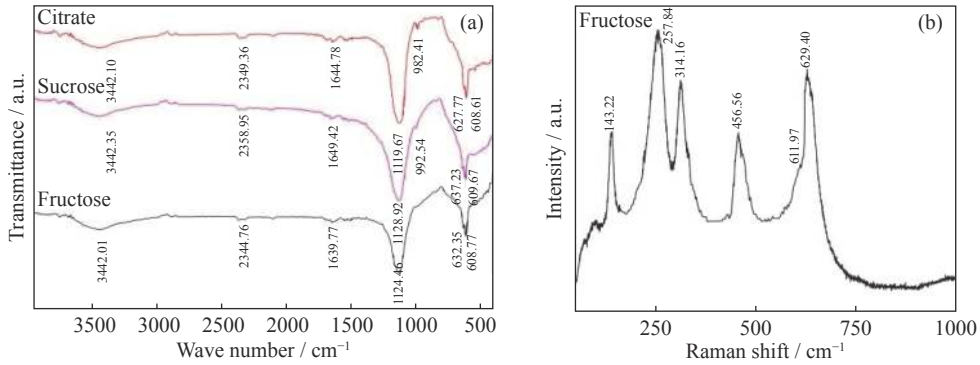

Fig. 5. (a) FT-IR spectra of the calcined nanopowders and (b) Raman spectrum of the heated fructose sample at 700°C.

3.5. Microstructural features and morphology

Figs. 6(a) and 6(b) show the FE-SEM micrograph and morphology of the citrate sample calcined at 700°C for 1 h, respectively. The abrupt combustion of nitrate radicals and the high-temperature combustion of citric acid, which were previously observed in the related DTA graph (Fig. 2(a)), resulted in the partial agglomeration of the synthesized particles (Fig. 6(a)) [32,37]. Meanwhile, the grains (Fig. 6(b)) and crystallite sizes (Table 3) were retained in the nanoscale. Fig. 7 illustrates the morphological features of the individual particles of the sucrose sample heated at 700°C. As these particles were smaller than 100 nm, the XRD pattern (Fig. 3) showed the simultaneous presence of monoclinic and tetragonal phases in the sucrose sample [9]. Electron micro-

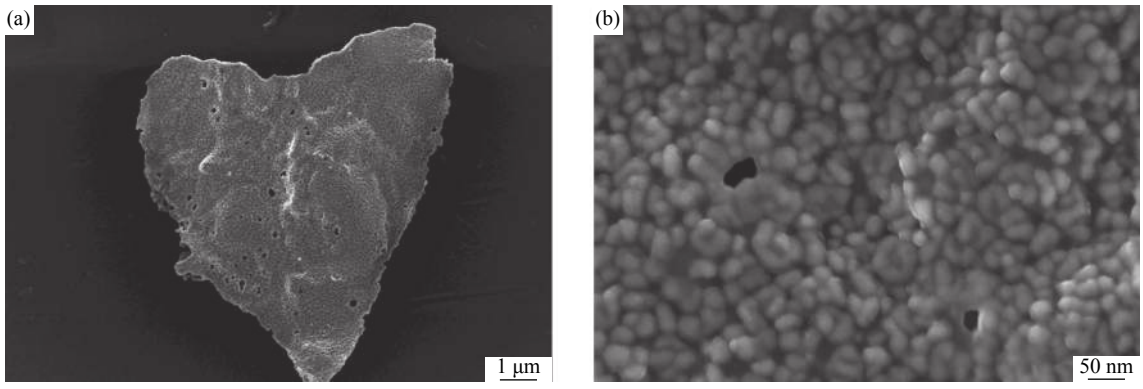

Fig. 6. (a) SEM micrograph and (b) morphology of the citrate sample calcined at 700°C.

graphs of the sample prepared using fructose as chelating agent and calcined at 700°C are presented in Fig. 8. No sign of agglomeration was detected in Fig. 8(a), and the pure tetragonal zirconia phase with the particle size of <40 nm (Table 5) and crystallite size of <23 nm (Table 3) was obtained after calcination at 700°C. Fig. 8(b) illustrates the morphology of some individual synthesized tetragonal particles. For the fructose-based sample heated at 700°C, tetragonal zirconia is the only phase. As the preferable crystal growth direction of this structure is along the *c*-axis, it is expected to result in hexagonal prisms or rod-shaped crystals in the microstructure [34]. Although the growth of the tetragonal zirconia phase seems to result in a uniaxial shape, the particles are not observed to have either an increased width or an agglomerated form. In this figure, the crystal growth direction along the *c*-axis is clear, which is consistent with the results shown in Fig. 4.

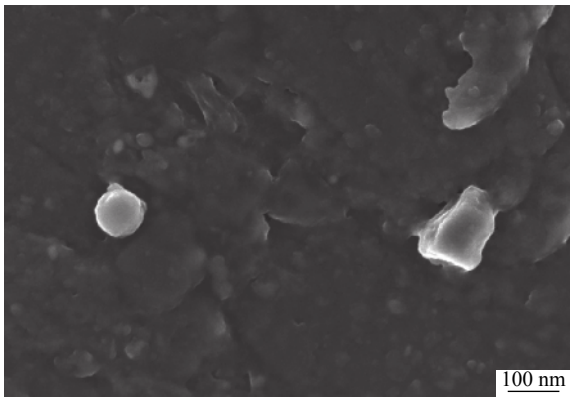

Fig. 7. SEM micrograph of the sucrose sample calcined at 700°C.

Majedi *et al.* [38] investigated the green synthesis of zirconia nanoparticles using zirconium acetate and lemon juice and detected the cubic phase of zirconia with the particle size of <20 nm. Ray *et al.* [10] reported the production of 1mol%, 2mol%, and 5mol% Cr^{3+}-doped nano-sized zirconia and investigated the phase stability by XRD. They claimed that, with the addition of Cr^{3+} cations, cubic zirconia would be stabilized at 600°C. In the case of nano-zirconia, the XRD pattern of the tetragonal phase becomes more similar to that of the cubic phase [3]. A small shoulder at 2θ of 59.4° (Fig. 3) is the distinguishing characteristic of the tetragonal phase from the cubic phase of zirconia. However, when the crystallite size of the tetragonal phase becomes smaller than 30 nm, the shoulder would be located lower than the main peaks, which would result in the detection of the cubic phase instead of the tetragonal phase [39–40]. The main characteristic crystallographic plane of the tetragonal phase is (102), which has not been detected by XRD (Fig. 3). In the current study, the electron diffraction pattern helped detect the (102) plane. The transmission electron micrograph (TEM) and selected area electron diffraction (SAED) pattern of the fructose sample calcined at 700°C are presented in Figs. 9(a) and 9(b), respectively, which confirmed the formation of tetragonal zirconia phase in the fructose sample.

From Fig. 9(a), the crystallite size of <9 nm is observed in this sample, which is close to the data calculated using the Scherrer equation (Table 3). Measuring the (*hkl*) index from the electron diffraction patterns is possible [41]. For each circle, the specific radius is calculated using Eq. (7):

$$Rd_{hkl} = L\lambda \tag{7}$$

where L is the camera constant (L = 0.1 nm), R is the radius of the circle (nm), λ is the electron beam wavelength (λ = 0.21658 nm), and d_{hkl} is the distance of planes (nm). For the (101) crystalline plane of the fructose sample, this distance was calculated to be 0.293174 nm. From Fig. 9(b), for the most interior circle, which has the maximum plane distance, d_{hkl} is calculated to be equal to 0.293279 nm. Thus, the structure of zirconia should be tetragonal or cubic. However, the calculation of the other distances showed that the values are closer to the values of the tetragonal phase; especially, the inset electron diffraction pattern in Fig. 9(b) indicates the existence of the (102) crystalline plane, which is specific to the tetragonal phase but not present in the cubic phase [29,34]; therefore, it was considered the tetragonal zirconia phase in this sample.

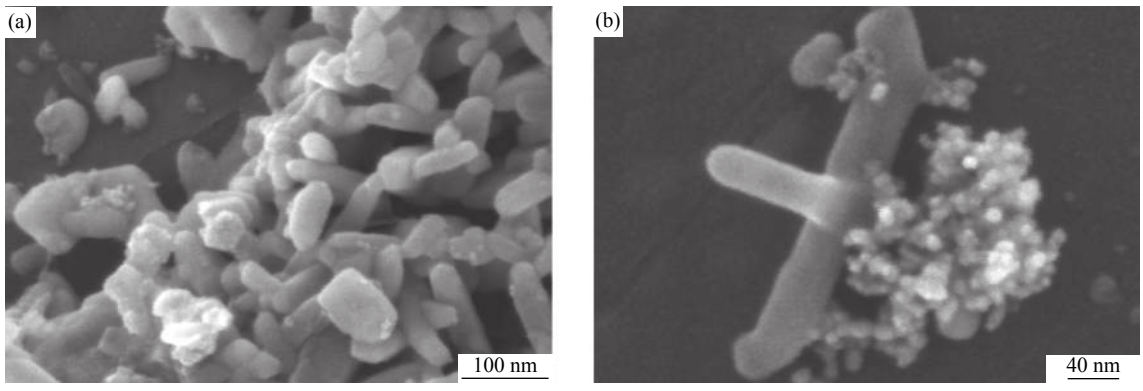

Fig. 8. (a) SEM micrograph and (b) morphology of some individual tetragonal particles in the fructose sample calcined at 700°C.

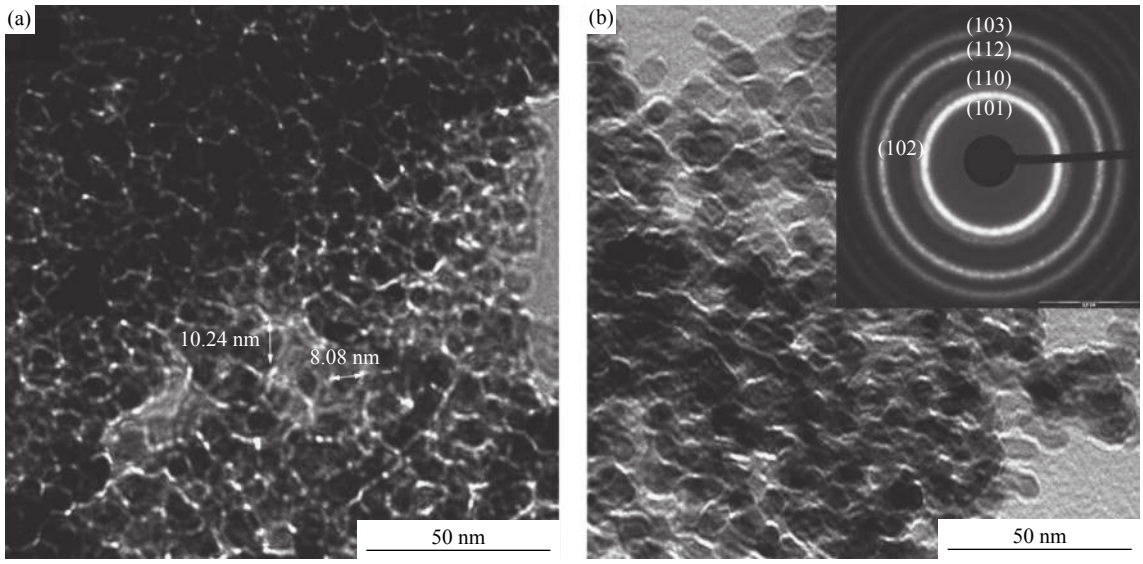

Fig. 9. (a) Transmission electron micrograph and (b) selected area electron diffraction pattern of the fructose sample calcined at 700°C.

4. Conclusion

In this study, the synthesis of stabilized nano-tetragonal zirconia was investigated via Pechini and sugar-based methods using zirconium hydroxide, citric acid, sucrose, and fructose after calcination at 500, 600, and 700°C in air. The effects of heat treatment and chelating agents on the thermal behavior, physical phase, and microstructural properties were investigated. The main findings of the research can be summarized as follows:

(1) From the diffraction data, mixtures of monoclinic and tetragonal phases were observed for the sucrose and citrate samples at 600 and 700°C. In the fructose sample, the tetragonal structure was the unique characterized phase. Moreover, no trace of the amorphous phase was observed in the phase composition of these samples. The crystallite sizes of the tetragonal phase were determined for the citrate (21.4 nm), sucrose (15.9 nm), and fructose (22.9 nm) samples after calcination at 700°C.

(2) Using the BET methods, the particle sizes were measured to be ≤50 nm for all samples after calcination at 700°C. These results are consistent with the microstructural and morphological observations by electron microscopy.

(3) The tetragonality of the crystal structure was indicated by the presence of the (102) crystalline plane in the selected area electron diffraction pattern of the fructose sample calcined at 700°C. The crystallite sizes obtained from the TEM micrographs (8–11 nm) were close to the calculated crystallite sizes obtained from the XRD and Scherrer equation (23 nm) for this sample.

(4) Using fructose as chelating agent seems to be a more effective route to produce the pure stabilized tetragonal zirconia phase at a lower temperature of 500°C. The use of zirconium hydroxide rather than zirconium alkoxides or salts as precursor is also expected to make this process green and cost-effective.

References

[1] F. Petrakli, M. Arkas, and A. Tsetsekou, α-alumina nanospheres from nano-dispersed boehmite synthesized by a wet chemical route, *J. Am. Ceram. Soc.*, 101(2018), No. 8, p. 3508.

[2] K. Agilandeswari and A.R. Kumar, Optical, electrical properties, characterization and synthesis of $Ca_2Co_2O_5$ by sucrose assisted sol–gel combustion method, *Adv. Powder Technol.*, 25(2014), No. 3, p. 904.

[3] C. Suciu, A.C. Hoffmann, A. Vik, and F. Goga, Effect of calcination conditions and precursor proportions on the properties of YSZ nanoparticles obtained by modified sol–gel route, *Chem. Eng. J.*, 138(2008), No. 1-3, p. 608.

[4] K. Prabhakaran, A. Melkeri, N.M. Gokhale, and S.C. Sharma, Synthesis of nanocrystalline 8mol% yttria stabilized zirconia powder from sucrose derived organic precursors, *Ceram. Int.*, 33(2007), No. 8, p. 1551.

[5] Y.J. Wu, A. Bandyopadhyay, and S. Bose, Processing of alumina and zirconia nano-powders and compacts, *Mater. Sci. Eng. A*, 380(2004), No. 1-2, p. 349.

[6] P.S. Behera, S. Bhattacharyya, and R. Sarkar, Effect of citrate to nitrate ratio on the sol–gel synthesis of nanosized α-Al_2O_3 powder, *Ceram. Int.*, 43(2017), No. 17, p. 15221.

[7] R.E. Juárez, D.G. Lamas, G.E. Lascalea, and N.E.W. de Reca, Synthesis of nanocrystalline zirconia powders for TZP ceramics by a nitrate–citrate combustion route, *J. Eur. Ceram. Soc.*, 20(2000), No. 2, p. 133.

[8] J. Yang, J.S. Lian, Q.Z. Dong, Q.F. Guan, J.W. Chen, and Z.X. Guo, Synthesis of YSZ nanocrystalline particles via the nitrate–citrate combustion route using diester phosphate (PE) as dispersant, *Mater. Lett.*, 57(2003), No. 19, p. 2792.

[9] K.A. Singh, L.C. Pathak, and S.K. Roy, Effect of citric acid on the synthesis of nano-crystalline yttria stabilized zirconia powders by nitrate–citrate process, *Ceram. Int.*, 33(2007), No. 8, p. 1463.

[10] J.C. Ray, P. Pramanik, and S. Ram, A novel polymer matrix method for synthesizing ZrO_2 nanocrystals at moderate temperature, *J. Mater. Sci. Lett.*, 20(2001), p. 2017.
[11] A. Majedi, F. Davar, and A. Abbasi, Sucrose-mediated sol–gel synthesis of nanosized pure and S-doped zirconia and its catalytic activity for the synthesis of acetyl salicylic acid, *J. Ind. Eng. Chem.*, 20(2014), No. 6, p. 4215.
[12] H.Y. Zhu, B. Liu, M.M. Shen, Y. Kong, X. Hong, Y.H. Hu, W.P. Ding, L. Dong, and Y. Chen, Effect of maltose for the crystallization of tetragonal zirconia, *Mater. Lett.*, 58(2004), No. 25, p. 3107.
[13] F. Heshmatpour and R.B. Aghakhanpour, Synthesis and characterization of nanocrystalline zirconia powder by simple sol–gel method with glucose and fructose as organic additives, *Powder Technol.*, 205(2011), No. 1-3, p. 193.
[14] R.D. Purohit, S. Saha, and A.K. Tyagi, Combustion synthesis of nanocrystalline ZrO_2 powder: XRD, Raman spectroscopy and TEM studies, *Mater. Sci. Eng. B*, 130(2006), No. 1-3, p. 57.
[15] M.M. Rashad and H.M. Baioumy, Effect of thermal treatment on the crystal structure and morphology of zirconia nanopowders produced by three different routes, *J. Mater. Process. Technol.*, 195(2008), No. 1-3, p. 178.
[16] F. Maglia, M. Dapiaggi, I. Tredici, B. Maroni, and U. Anselmi-Tamburini, Synthesis of fully dense nanostabilized undoped tetragonal zirconia, *J. Am. Ceram. Soc.*, 93(2010), No. 7, p. 2092.
[17] F. Davar, A. Hassankhani, and M.R. Loghman-Estarki, Controllable synthesis of metastable tetragonal zirconia nanocrystals using citric acid assisted sol–gel method, *Ceram. Int.*, 39(2013), No. 3, p. 2933.
[18] V.V. Srdić, M. Winterer, and H. Hahn, Sintering behavior of nanocrystalline zirconia prepared by chemical vapor synthesis, *J. Am. Ceram. Soc.*, 83(2004), No. 4, p. 729.
[19] N. Nafsin, H. Li, E.W. Leib, T. Vossmeyer, P. Stroeve, and R.H.R. Castro, Stability of rare-earth-doped spherical yttria-stabilized zirconia synthesized by ultrasonic spray pyrolysis, *J. Am. Ceram. Soc.*, 100(2017), No. 10, p. 4425.
[20] J. Joo, T. Yu, Y.W. Kim, H.M. Park, F.X. Wu, J.Z. Zhang, and T. Hyeon, Multigram scale synthesis and characterization of monodisperse tetragonal zirconia nanocrystals, *J. Am. Chem. Soc.*, 125(2003), No. 21, p. 6553.
[21] N. Chandra, D.K. Singh, M. Sharma, R.K. Upadhyay, S.S. Amritphale, and S.K. Sanghi, Synthesis and characterization of nano-sized zirconia powder synthesized by single emulsion-assisted direct precipitation, *J. Colloid Interface Sci.*, 342(2010), No. 2, p. 327.
[22] U.K.H. Bangi, C.S. Park, S. Baek, and H.H. Park, Sol–gel synthesis of high surface area nanostructured zirconia powder by surface chemical modification, *Powder Technol.*, 239(2013), p. 314.
[23] S. Shukla, S. Seal, R. Vij, and S. Bandyopadhyay, Effect of HPC and water concentration on the evolution of size, aggregation and crystallization of sol–gel nano zirconia, *J. Nanopart. Res.*, 4(2002), p. 553.
[24] C. Suchomski, D.J. Weber, P. Dolcet, A. Hofmann, P. Voepel, J. Yue, M. Einert, M. Möller, S. Werner, S. Gross, I. Djerdj, T. Brezesinski, and B.M. Smarsly, Sustainable and surfactant-free high-throughput synthesis of highly dispersible zirconia nanocrystals, *J. Mater. Chem. A*, 5(2017), No. 31, p. 16296.
[25] F. Kazemi, S. Sohrabi, S. Malek-Ahmadi, H.R. Rezaie, and S.R. Allahkaram, Synthesis of metastable tetragonal zirconia nanopowder during extraction of zirconia from zircon by alkaline fusion process, [in] *The International Conference on Ultrafine Grained and Nanostructured Materials*, Tehran, Iran, 2007, p.75.
[26] R. Jenkins and R.L. Snyder, *Introduction to X-Ray Powder Diffractometry*, 2nd ed., John Wiley & Sons, New York, 2012, p. 25.
[27] A. Saberi, B. Alinejad, Z. Negahdari, F. Kazemi, and A. Almasi, A novel method to low temperature synthesis of nanocrystalline forsterite, *Mater. Res. Bull.*, 42(2007), No. 4, p. 666.
[28] M. Bashir, S. Riaz, Z.N. Kayani, S. Naseem, Synthesis of bone implant substitutes using organic additive based zirconia nanoparticles and their biodegradation study, *J. Mech. Behav. Biomed. Mater.*, 88(2018), p. 48.
[29] K.A. Aly, N.M. Khalil, Y. Algamal, and Q.M.A. Saleem, Estimation of lattice strain for zirconia nano-particles based on Williamson-Hall analysis, *Mater. Chem. Phys.*, 193(2017), p. 182.
[30] C.J. Szepesi and J.H. Adair, High yield hydrothermal synthesis of nano-scale zirconia and YTZP, *J. Am. Ceram. Soc.*, 94(2011), No. 12, p. 4239.
[31] J.C.D. da Costa, S. Coombs, J. Lim, and G.Q. Lu, Characterization of xerogels derived from sucrose templated sol–gel synthesis, *J. Sol–Gel Sci. Technol.*, 31(2004), No. 1-3, p. 215.
[32] R. Mahendran, S.P.K. Babu, S. Natarajan, S. Manivannan, and A. Vallimanalan, Phase transformation and crystal growth behavior of 8mol% ($SmO_{1.5}$, $GdO_{1.5}$, and $YO_{1.5}$) stabilized ZrO_2 powders, *Int. J. Miner. Metall. Mater.*, 24(2017), No. 7, p. 842.
[33] Y.L. Zhang, X.J. Jin, Y.H. Rong, T.Y. Hsu, D.Y. Jiang, and J.L. Shi, The size dependence of structural stability in nano-sized ZrO_2 particles, *Mater. Sci. Eng. A*, 438-440(2006), p. 399.
[34] F. Kazemi, A. Saberi, S. Malek-Ahmadi, S. Sohrabi, H.R. Rezaie, and M. Tahriri, A novel method for synthesis of metastable tetragonal zirconia nanopowders at low temperatures, *Ceram. Silik.*, 55(2011), No. 1, p. 26.
[35] C.C. Koch, *Nanostructured Materials, Processing, Properties and Potential Applications*, William Andrew, New York, 2002, p. 4.
[36] R.N. Das, A. Bandyopadhyay, and S. Bose, Nanocrystalline α-Al_2O_3 using sucrose, *J. Am. Ceram. Soc.*, 84(2004), No. 10, p. 2421.
[37] A. Srivastava and M.K. Dongare, Low-temperature preparation of tetragonal zirconia, *Mater. Lett.*, 5(1987), No. 3, p. 111.
[38] A. Majedi, A. Abbasi, and F. Davar, Green synthesis of zirconia nanoparticles using the modified Pechini method and characterization of its optical and electrical properties, *J. Sol–Gel Sci. Technol.*, 77(2016), No. 3, p. 542.
[39] E. Djurado and E. Meunier, Synthesis of doped and un-doped nano powders of tetragonal polycrystalline zirconia (TPZ) by spray-pyrolysis, *J. Solid State Chem.*, 141(1998), No. 1, p. 191.
[40] A. Bumajdad, A.A. Nazeer, F.A.I. Sagheer, S. Nahar, and M.I. Zaki, Controlled synthesis of ZrO_2 nanoparticles with tailored size, morphology and crystal phases via organic/inorganic hybrid films, *Sci. Rep.*, 8(2018), art. No. 3695.
[41] X. Zou, S. Hovmöller, and P. Oleynikov, *Electron Crystallography: Electron Microscopy and Electron Diffraction*, Oxford University Press, Oxford, 2011, p. 98.